JOURNAL OF SPACECRAFT AND ROCKETS
Vol. 37, No. 1, January–February 2000

Solar Absorber Plates: Design and Application to Microgravity Capillary-Pumped-Loop Experiments

M. B. H. Mantelli* and E. Bazzo†
Federal University of Santa Catarina, 88040-900 Florianópolis, Brazil

An absorber plate is proposed to collect solar energy to be supplied to experiments in space. Its performance depends on the geometry of the satellite, on the incident environmental heat loads (solar, albedo, and Earth infrared radiation), and on the temperature level of the plate, which is usually an outcome of the microgravity experiment. A steady-state mathematical model is proposed to estimate the temperature distribution along the plate. Finite difference numerical models are developed for the steady-state and transient conditions and compared with the analytical model. Average temperatures and the net heat absorbed are determined. An experimental setup is developed to generate data to be compared with the theoretical models. A good agreement is observed among the experimental data, the analytical, and the numerical results. The procedure is applied to the small-scale capillary-pumped-loop experiment, which will fly aboard the French Brazilian Microsatellite. This experiment is described. Solar absorbers can be considered as a reliable alternative to improve the available heat power for experiments in space.

Nomenclature

a	= half the length of the capillary pump, m
B	= bias error
b	= half the length of the border of the plate, x direction, m
C_n, CC_n	= integration constant (n variable)
Cp	= specific heat, constant pressure, kW/kg · K
c	= half the length of the border of the plate, y direction, m
df	= degrees of freedom
h_r	= radiative heat transfer coefficient, W/m^2 · K
k	= thermal conductivity, W/m · K; time-iteration counting variable
m, n	= node numbering (x and y directions, respectively)
N	= maximum number of series terms, number of elements
P	= electrical power, W
q	= thermal power, W/m^2
R	= electrical resistance, Ω
S	= environmental total heat load, W/m^2; standard deviation
T	= temperature, K
T_f	= fluid temperature, K
T_s	= space temperature, K
t	= thickness of the plate, m; time, s; Student t multiplying factor
U	= uncertainty interval
V	= voltage, V
x, y, z	= orthogonal directions, Cartesian system
α	= absorptivity
ϵ	= emissivity
$\theta, \Theta, \Phi, \Psi$	= temperature difference, $(T - T_f)$
λ, μ	= eigenvalue
ρ	= density, kg/m^3
σ	= Stefan–Boltzmann constant, 5.67×10^{-8} W/m^2 · K^4

Received 26 September 1998; revision received 1 June 1999; accepted for publication 22 July 1999.

*Professor, Satellite Thermal Control Laboratory/Mechanical Engineering Department, Mathematics Department, CP 476; marcia@labsolar.ufsc.br. Member AIAA.

†Professor, Satellite Thermal Control Laboratory, Mechanical Engineering Department, CP 476; ebazzo@emc.ufsc.br.

Introduction

IN the past decade, especially after the end of the cold war, many countries have had easier access to the spacecraft technologies. They are now able to run their space programs more efficiently than before. On the other hand, it is well known that the budgets for space programs have, in general, decreased. To adapt the space programs to these budgets, a new generation of small satellites is being developed. One of the challenges in the development of small satellites is to create new thermal control technologies or to adapt the existing ones, because, as the satellite reduces in size, the heat dissipation per unit volume increases.

Most of the satellites under development within the frame of the Brazilian Space Program have equatorial orbits and are small in size, such as the French Brazilian Microsatellite planned to be launched in 2001. Several scientific and technological experiments will be tested aboard this satellite. The Satellite Thermal Control Group of the Federal University of Santa Catarina proposed to the Brazilian Academy of Sciences a small-scale capillary-pumped-loop (CPL) experiment, which was approved.

The available power for experiments in space in small spacecrafts is usually limited. In this work theoretical and experimental results are presented for an absorber plate, proposed to collect solar energy to be used in experiments under microgravity such as the small-scale CPL.

A CPL is a passive two-phase heat-transfer loop that is able to transport an amount of energy one order of magnitude larger than heat pipes. With the increase of the heat dissipation per unit volume in spacecrafts along the years, CPL has been more and more considered as a good alternative for the thermal control of satellites. A basic CPL has the following main components: one or more cold plates, where dissipating elements are installed and where evaporators (one or more) are thermally connected; a condenser to transfer heat from the working fluid to the heat rejection system; smooth tubes, for the transportation of the vapor generated in the evaporators to the condenser; smooth tubes for the transportation of the liquid, which leaves the condenser to the evaporator; and a fluid reservoir, to control the amount of liquid in the loop and to control the fluid operation temperature.

The basic CPL operating principle is summarized as follows[1]: as the evaporator is heated, liquid from the saturated wick evaporates, and the vapor flows through the loop to the condenser zone, where heat is removed and vapor is condensed; from the condenser, the liquid flows back to the evaporator by capillary action. Before leaving the condenser, any remaining vapor bubble is collapsed in the subcooled liquid return line. Unlike conventional heat pipes CPL has the wick structure only in the evaporator section and provides

individual lines for liquid and vapor flows. These features allow a high capillary pumping rate with homogeneous wick structures. As in a heat pipe, the meniscus self-adjusts to establish the pumping action needed to match the flow losses along the loop.

Literature Review

In the past two decades researchers around the world have studied several aspects of CPLs. Theoretical and experimental studies dealing with the complete system or with specific CPL components, such as capillary pumps, condensers, and reservoirs, have been published. A brief summary of the prototypes tested under microgravity conditions are presented here, with special attention to the experiment energy supply systems employed.

Most of the microgravity tests of CPLs were carried on the space shuttles. Small-scale CPLs were tested inside the GAS (get away special) cylindrical container. This is the case of the CPL1,[2] tested in June 1985, and of the European TPX (two-phase experiment),[3] tested in February 1994. The power was supplied by batteries, which were experiment dedicated and located inside the container.

Larger CPL prototypes were tested using the U.S. Space Shuttle Hitchhiker Carrier System. In these cases the power necessary to run the experiments was supplied by the shuttle. The following six different CPL experiments were microgravity tested under these conditions: the CPL1 (a reflight of the CPL1/GAS in January 1986)[1]; the CAPL1,[4] flown in February 1994; the CAPL2,[5] flown in September 1995; the TPF (two-phase flow),[6] tested in August 1997; and the loop heat pipe (LHP),[7] tested in December 1997. CPL are still in development in the United States, and new prototypes are scheduled to be tested in the near future in microgravity conditions,[8] using the space shuttle facilities.

The world interest in the development of LHP is growing nowadays, especially in the United States. Actually, the former USSR developed, in the last decade, an advanced program in LHP, which is a simpler conception of CPLs. The main difference between CPLs and LHPs is in the reservoir that is a compensation chamber in the LHP. Maidanik et al.[9] described several LHPs, with special emphasis in the ALYONA module, which was developed for tests aboard the spacecraft GRANAT launched in December 1989. This system used solar energy as the heat source and thermal radiation to space as the heat sink. A controller, developed especially for these tests, controlled the amount of heat radiated to the space. In space the LHP transferred 40–50 W of heat power for an absorber plate area of 0.48 m^2. The experiment was considered well succeeded by the authors, but details of the system design, of the techniques employed, of the physical, analytical, and/or numerical models adopted and the data collected are not available in the literature. Actually, LHP can be considered the state of art in Russia being presently used in its satellites, such as the OBZOR, launched in August 1994.[10]

In this work the solar energy is proposed as the heat source for the CPL and other experiments in space, providing test conditions for small satellites. Generally, small satellites do not have enough power available to run experiments in space and are not able to transport dedicated batteries because of weight limitations. This is the case of the French Brazilian Satellite.

Contributions

The Brazilian experiment, which will fly aboard the French Brazilian Satellite to be launched in 2001, consists of a small-scale CPL model, as reported.[11,12] The U.S. and European experimental models, especially those mounted and tested in the Space Shuttle GAS and Hitchhiker Systems, are, in fact, prototypes of CPLs designed to transport large heat loads. The Brazilian CPL is conceptually small and designed to transfer an amount of heat compatible with the size of the Brazilian satellites. CPLs present geometric flexibility, which is a very useful characteristic for the thermal control of satellites, when compared to heat pipes. Therefore, one attempt of the CPL study in Brazil is to combine its flexibility with the heat capacity necessity of the Brazilian satellites. Another objective is to test capillary pumps with a porous element made of sintered nickel powder, not tested in orbit yet. More information about CPL development in Brazil can be found in Refs. 11 and 12.

Most of the CPL experiments in the world were tested aboard the space shuttle, which is a large spacecraft and provides several test facilities. In these cases the weight of the setup is not a strong constraint. This is not the case of the French Brazilian Satellite, where the weight and the available power are severe limitations for the experiment. To solve these problems, the use of solar energy absorbed by a plate is proposed and applied to the small-scale CPL experiment. The analytical, numerical, and experimental analysis of this plate is presented. The proposed absorber plate is designed to attend the needs of the CPL experiment, but the concept, the mathematical model, and the numerical techniques are general and can be easily adopted to other cases.

CPL Experiment Description

Figure 1 presents a schematic of the French Brazilian Satellite geometry, with the location of the small-scale CPL experiment. The CPL basically consists of one solar absorber plate, one radiator plate, and one reservoir. The absorber plate collects the thermal solar energy and delivers it to the capillary pump, which is attached to its center. The thermal energy, as latent heat, is transferred to the radiator plate, where it is released into space. The capillary-pump structure consists of a tubular sintered nickel powder, with a porosity of 50% and an effective capillary radius in the range of 3–8 μm. The fluid selected is ammonia.

The geometry and weight of the satellite are severe limitations in the experiment. The total mass of the experiment must be up to 3 kg. Because of the geometry of the satellite, the maximum possible size of the absorber plate is 0.2×0.2 m (0.04 m^2) and of the radiator plate is 0.55×0.25 m. The surface finishing of plates must provide, to the absorber, the maximum capacity of absorption of solar energy and, to the radiator, the maximum capacity of rejection of radiative heat in the infrared spectrum. Because of its simplicity of application and availability in the market, black and white paints are selected for the absorber and radiator plates, respectively. Conservative values of the emissivity and absorptivity of black paints, used in this work, are $\epsilon = \alpha = 0.85$. For the white paint these values are $\epsilon = 0.84$ and $\alpha = 0.15$.

The absorber and radiator plates are made of 1-mm thick aluminum sheets. Stainless-steel tubes of an external diameter of 0.0048 m ($\frac{3}{16}$ in.) are used to connect the capillary pump to the radiator. The reservoir consists of a 0.019-m ($\frac{3}{4}$ in.)-diam stainless-steel cylinder, with 40 ml of volume.

In Ref. 12, a steady-state heat balance for the whole experiment is presented, using lumped-plate temperatures. The optimal range of temperature is between 275 and 290 K. For these conditions the CPL experiment is able to transfer the absorbed solar energy plus 15 W of electrical power, to be supplied by the satellite. The reservoir controls the fluid temperature and, therefore, the temperature levels of the absorber and radiator plates. The surface temperature levels determine the plate capacity of absorbing and rejecting heat. For these calculations the CPL was considered a perfect conductor.

Satellite Orbit and Environmental Heat Load

The environmental heat loads over the satellite are a direct function of its orbit. The satellite orbit is equatorial and elliptic, with period of 98 min, with 1000 km of apogee, 400 km of perigee, and 7 deg of inclination. Figure 1 also shows a schematic of the orbit and of the satellite attitude, which is sun-synchronous. The satellite yz

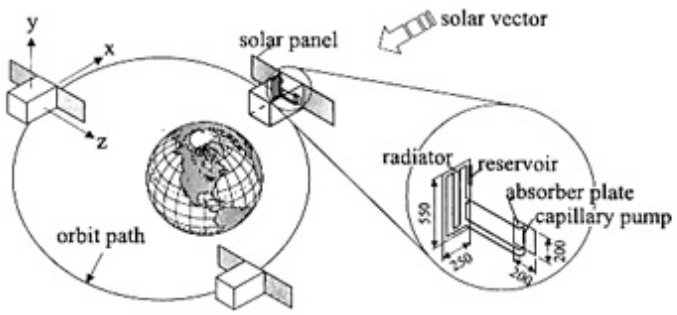

Fig. 1 Schematic of the French Brazilian Satellite orbit, attitude, and CPL experiment.

plane is always pointed out to the sun, whereas the y axis is aligned with the normal to the ecliptic plan.

According to Gilmore,[13] the solar, the Earth infrared, and the Earth's albedo radiations are the main sources of environmental heat loads. Direct solar radiation is the largest source of heat incident on the satellite. Because of the Earth's elliptical orbit, the solar radiation that reaches the Earth varies approximately ±3.5%, ranging from 1300 W/m^2 at the summer solstice to a maximum of 1400 W/m^2 at the winter solstice. The absorber always receives solar energy, except for the period of the orbit when the satellite is in the Earth's shadow. Figure 2 presents the solar, the Earth infrared, the Earth's albedo, and the total environmental heat loads over the absorber plate for 1 January. Details of the calculation are given by Couto and Mantelli.[14] This figure shows that the total heat load curves can be assumed as a step function. The total heat load, for the shadowed and sunny part of the orbit, can be taken as constant values of 356 and 1444.7 W/m^2, respectively, for the absorber area of 0.2 × 0.2 m. In one orbit the satellite is in the Earth's shadow during 34 min and under solar radiation during 64 min. The total environmental heat load as a function of time is required to estimate the heat to be transferred by the experimental CPL.

Mathematical Model

Figure 3 shows the physical model used for the mathematical formulation of the problem, including the boundary conditions. The temperature distribution is given by the solution of a steady-state, two-dimensional, and nonhomogeneous boundary condition problem with uniform internal heat absorption, which is not available in the literature. This model was developed for the present CPL program and is briefly presented here. More details can be found in the paper of Mantelli and Bazzo.[15]

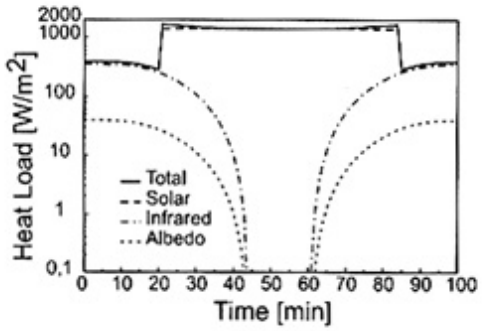

Fig. 2 Environmental heat loads over the absorber plate as a function of time.

Because of the nonhomogeneous boundary conditions, the heat problem is divided into two domains (Fig. 3). Following a procedure suggested by Arpaci,[16] each domain, in turn, is divided in two other problems with a known solution: a two-dimensional problem without heat generation and a one-dimensional problem with heat generation. The solution is the combination of all of these four solutions, according to their interface boundary conditions. No solution could be obtained if the choice of the one-dimensional heat problem direction were the same for both domains.

In Fig. 3 the absorber is considered insulated at its edges. The plate is rectangular with dimensions: $2b$ and $2c$ in the x and y directions, respectively. The thickness of the plate is t. The capillary pump is assumed to be located exactly at the center of the plate in the x direction. The length of the capillary pump is $2a$. As the problem is symmetric with relation to the x and y axes, only one-fourth of the plate is modeled. This figure also shows the two domains. The temperature difference between the plate and the capillary pump is assumed to be $\Theta(x, y)$ for domain 1 and $\Psi(x, y)$ for domain 2. The temperature of the capillary pump is assumed to be equal to the fluid temperature T_f. The contact resistance between the plate and the capillary pump is considered zero.

The heat partial differential equation, which describes the temperature distribution along the plate, is, for domain 1,

$$\frac{\partial^2\Theta}{\partial x^2} + \frac{\partial^2\Theta}{\partial y^2} + \frac{q}{k\,t} = 0 \tag{1}$$

This equation is subjected to the boundary conditions shown in Fig. 3.

The radiative heat exchanged among the plate, the sun, and the space is calculated using the plate mean temperature $\bar{T}$, which is so assumed because the variation of the temperature along the plate is not expected to be large. Also, the optical properties (absorptivity and emissivity) do not vary much for small temperature gradients along the plate. Therefore, the net heat absorbed was considered uniformly distributed along the surface of the absorber plate, given by a constant value q, which is calculated using the Stefan–Boltzmann equation for radiation heat transfer:

$$q = \alpha S - \epsilon\sigma\left(\bar{T}^4 - T_s^4\right) \tag{2}$$

The determination of q is iterative. Its value is first guessed, the temperature distribution is determined, the temperature average is obtained, and q is calculated again until the convergence is achieved.

The heat-conduction problem in each domain, composed of a two-dimensional problem with no environmental heat load and by

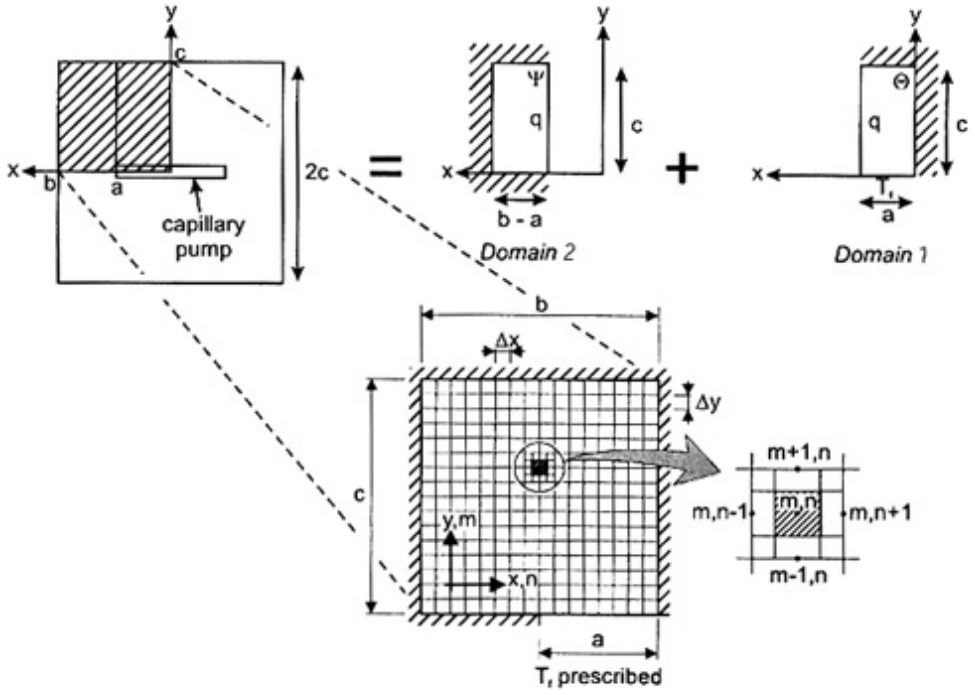

Fig. 3 Absorber plate physical model and grid scheme.

Table 1 Geometric and thermophysical properties of the absorber plate

Parameter	Value
a	0.05 m
b	0.1 m
c	0.1 m
t	0.001 m
k	177 W/mK
ϵ	0.85
α	0.85
T_f	280 K
T_s	4 K
q	1444.7 W/m^2

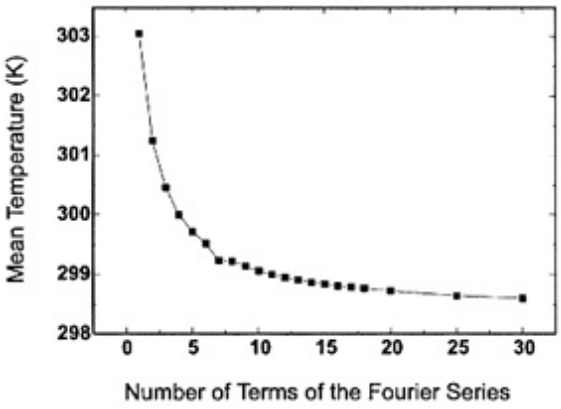

Fig. 4 Absorber plate mean temperature as a function of the number of the Fourier series terms.

a one-dimensional problem with a uniform absorption of the environmental heat load, for domain 1 is

$$\Theta(x, y) = \theta(x, y) + \Phi(y) \tag{3}$$

The temperature distribution, obtained by the solution of Eq. (3), after the application of the boundary conditions is given by

$$\Theta(x, y) = \sum_{n=0}^{\infty} C_{2n+1} \cosh(\lambda_{2n+1} x) \sin(\lambda_{2n+1} y) + \frac{1}{2}\frac{q}{kt}(-y^2 + 2cy) \tag{4}$$

where the eigenvalue λ_{2n+1} is

$$\lambda_{2n+1} = (2n + 1)\pi/2c \tag{5}$$

Similarly, the temperature distribution $\Psi(x, y)$ for domain 2 is

$$\Psi = \sum_{n=0}^{\infty} CC_n[\cosh(\mu_n x) - \tanh(\mu_n b)\sinh(\mu_n x)]\cos(\mu_n y) + \frac{q}{2kt}(-x^2 + 2bx + a^2 - 2ab) \tag{6}$$

where the eigenvalue μ_n is

$$\mu_n = n\pi/c \tag{7}$$

The C_n and CC_n constants need to be determined. The equality of temperatures and derivatives in the interface between domains 1 and 2 (see Fig. 3) results in two equations with the unknowns C_0, $C_1, \ldots, C_n$ and CC_0, $CC_1, \ldots, CC_n$. The orthogonality property of the Fourier series is applied to the two series, and a system of $2N$ equations in $2N$ unknowns is obtained. After the solution of this system, the resulting constants are substituted into Eqs. (4) and (6), and the temperature distribution is determined.

A study to determine the optimal number of Fourier series terms to be used in Eqs. (4) and (6) is performed. Figure 4 presents the mean-plate temperature obtained for several numbers of terms of the Fourier series. From this figure the conclusion can be made that

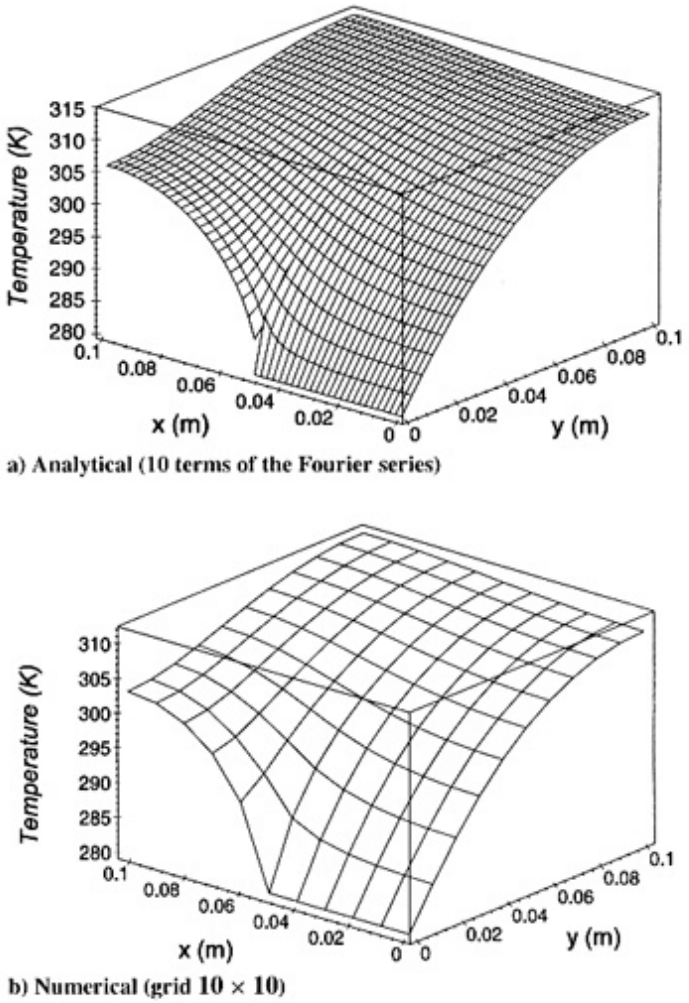

a) Analytical (10 terms of the Fourier series)

b) Numerical (grid 10×10)

Fig. 5 Steady-state temperature distributions.

10 terms are acceptable because of the precision and low computing time. Figure 5a presents the temperature distribution for one-fourth of the plate and for the geometric and physical data presented in Table 1, using 10 terms of the Fourier series.

Numerical Models

The finite difference technique is used for the numerical model of the solar absorber plate in steady-state and transient conditions. The same hypothesis adopted to the mathematical model and sketched in Fig. 3 is employed with the exception of the uniform heat absorption along the plate, not necessary for the numerical model. Again, only one-fourth of the plate is analyzed. Absolute temperatures are used in this model. Figure 3 also presents the plate grid scheme and the boundary conditions. Numerical models for steady-state and transient conditions are developed and presented.

Steady State

The finite difference equations are obtained from a heat balance between the heat coming from the neighbors' nodes by conduction and the heat exchanged with the environment by radiation. The radiation heat exchange, given by Eq. (2) introduces a nonlinearity in the heat balance equation. The linearized heat-transfer coefficient h_r is

$$h_r = \varepsilon\sigma\left(T^*_{m,n}\right)^3 \tag{8}$$

where $T^*_{m,n}$ is the temperature of the last iteration. A typical heat-balance equation for an inside node is

$$\left(2/\Delta x^2 + 2/\Delta y^2 + h_r/kt\right)T_{m,n} - \left[(T_{m,n-1} - T_{m,n+1})/\Delta y^2\right] - \left[(T_{m-1,n} - T_{m+1,n})/\Delta x^2\right] = \alpha S/kt \tag{9}$$

Similar heat balances are applied to all nodes of the plate, and the resulting system of $M \cdot N$ equations by $M \cdot N$ unknowns is solved applying the Gauss–Seidel iterative method.

Transient

The transient temperature distribution equation for an absorber plate receiving radiation heat over its surface is[17]

$$\frac{\partial^2 T}{\partial x^2} + \frac{\partial^2 T}{\partial y^2} + \frac{q}{kt} = \rho Cp \frac{\partial T}{\partial t} \tag{10}$$

The same grid scheme presented in Fig. 3 is considered. The fully implicit equation is used for the discretization in time. The heat-balance equation for an inside grid point is

$$\frac{\rho Cp}{k} \frac{T_{m,n}^{k+1} - T_{m,n}^{k}}{\Delta t} = \frac{T_{m,n-1}^{k} - 2T_{m,n}^{k} + T_{m,n+1}^{k}}{\Delta x^2}$$

$$+ \frac{T_{m+1,n}^{k} - 2T_{m,n}^{k} + T_{m-1,n}^{k}}{\Delta y^2} - \frac{\varepsilon\sigma T_{m,n}^{4k}}{k \cdot \Delta z} + \frac{\varepsilon\alpha S}{\Delta z} \tag{11}$$

Heat balances are applied to all nodes of the plate, resulting in a system of $M \cdot N$ equations by $M \cdot N$ unknowns. Because of the nonlinearities of the equations, direct methods cannot be applied to solve this system. The Gauss–Seidel point-by-point method is selected for its simplicity.

The average temperature of the plate and the net absorbed energy is obtained for the steady-state and transient conditions through the following expressions:

$$\bar{T} = \frac{\left(\sum_{n=1}^{N} \sum_{m=1}^{M} T_{m,n} \cdot \Delta x \cdot \Delta y\right)}{b \cdot c}$$

$$q = \frac{\left[\sum_{n=1}^{N} \sum_{m=1}^{M} \left(\alpha S - \varepsilon\sigma T_{m,n}^{4}\right) \cdot \Delta x \cdot \Delta y\right]}{b \cdot c} \tag{12}$$

Convergence Study

The steady-state results are important because they are used to calibrate the transient space grid and to compare with the transient results after the steady-state conditions are achieved. The steady-state results, in turn, are calibrated by the analytical model. To perform the convergence study, the plate is divided into different grids, and the mean temperature is determined for each grid. Figure 6 shows the mean temperature as a function of the number of grid elements in both directions (x and y) for two values of the tolerance (minimum acceptable temperature difference between two successive iterations): 10^{-3} and 10^{-4}. The behavior of both tolerance curves is similar for grids of up to 16×16 elements. After this limit the 10^{-3} tolerance curve is unstable. For the 10^{-4} tolerance curve the mean temperature is almost constant for grids of 10×10 elements or more. Therefore, the space grid 10×10 and tolerance of 10^{-4} are selected for the present work. The geometrical and thermophysical properties of the absorber plate, presented in Table 1, are used.

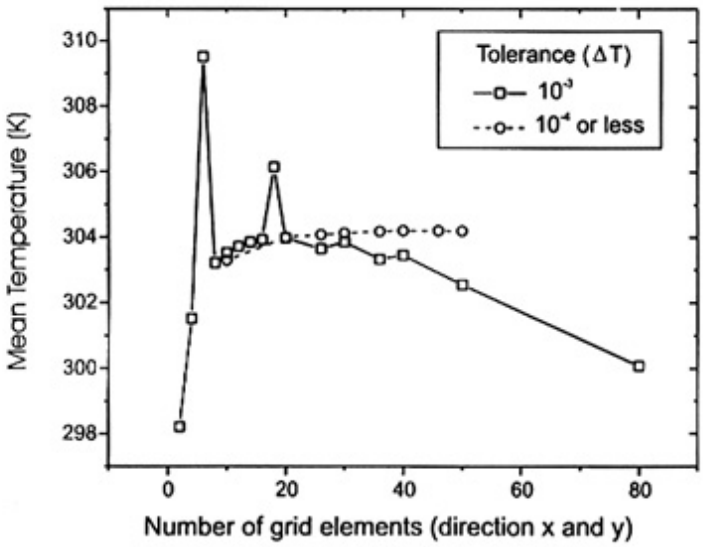

Fig. 6 Absorber plate mean temperature as a function of the number of grid elements in directions x and y, as given by the steady-state numerical model.

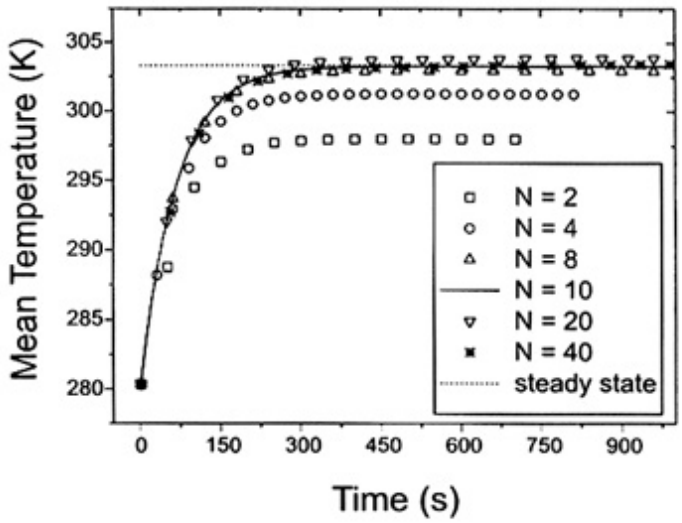

Fig. 7 Absorber plate mean temperature as a function of time for Δt = 1 s and different space grids.

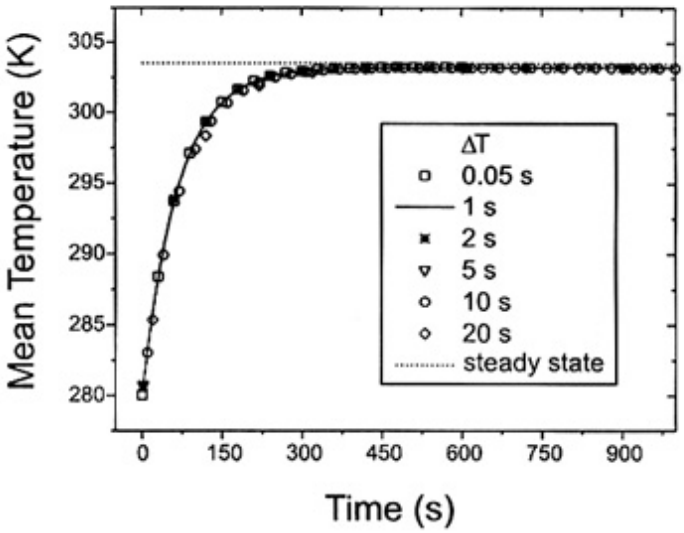

Fig. 8 Absorber plate mean temperature as a function of time for the 10×10 space grid and different time steps.

A similar study was performed for the transient case, where the space and the time grid refinements are considered. Based on the steady-state results, the tolerance used is 10^{-4}. Furthermore, the steady state is considered achieved when the relative temperature difference between two consecutive time iterations is less than 10^{-8} for all grid points. A $\Delta t = 1$ s time step is fixed, and the temperature distribution for several grids is obtained and plotted in Fig. 7. The steady-state temperature is also shown for comparison purposes. The number of nodes N in the x and y directions is the same. For $N \geq 8$ all of the curves are close, indicating that any mesh could be used. The grid 10×10 is selected, which is consistent with the steady-state study conclusion. Figure 7 also shows that the steady-state regime is achieved after around 450 s, starting from a uniform temperature (T_f level) initial condition.

The same procedure is adopted for the time-grid refinement study. For the 10×10 space grid several time steps are used to obtain curves of the mean temperature as a function of time presented in Fig. 8. All of the curves are similar, demonstrating that the mean temperature is not very sensitive to the time grid. The transient results are used in the comparison with experimental data, and the $\Delta t = 1$ s is selected as the ideal time grid.

Comparison Between Mathematical and Numerical Models

The mathematical model is implemented in a personal computer using a software of algebraic manipulation. The geometrical and

thermophysical properties used in this study are given in Table 1. Figure 5a shows the temperature distribution obtained for the absorber plate. The interface between the two domains (1 and 2; see Fig. 3) is observed in this figure. If more terms of the Fourier series were used, the smoother would be this interface. The temperature distribution obtained through the steady-state numerical model is presented in Fig. 5b for the 10 × 10 grid. The comparison between the steady-state analytical and numerical results shows that the temperature distribution obtained using both methods, mathematical and numerical, is very similar. The mathematical model predicts a larger temperature variation along the plate than the numerical model. This is expected because of the hypothesis of uniform heat absorption along the plate. Actually, the emitted energy increases at higher temperature regions, decreasing their temperature levels. Therefore, the numerical method is expected to present better results for the regions near the plate borders. On the other hand, the mathematical model is very useful for the design of the solar absorber plate and of the experiments, allowing easier parametric studies. For the present case both methods were shown to be precise and could be employed with no restrictions. The temperature distribution obtained using the numerical transient model after the steady-state regime is reached is exactly the same as the numerical steady-state model and is not presented.

Numerical Model for Transient State in One Complete Orbit

The numerical model developed for the study of the transient state is used. As shown in Fig. 2, the absorber plate is subjected to two different levels of total environmental heat loads, according to its position in orbit. The transition study is performed through the following procedure: the steady-state numerical model is used to determine the temperature distribution of the plate under the direct action of the solar radiation ($S = 1444.7$ W/m^2). This temperature distribution is used as the initial condition for the transient case. At instant zero the environmental heat loads drops instantaneously to $S = 356$ W/m^2. After 34 min the plate already achieved the steady-state conditions, and the satellite returns to the sunny portion of the orbit, where the environmental heat load instantaneously jumps back to $S = 1444.7$ W/m^2. The plate stays in this condition for 64 min, when it enters again the shadowed portion of the orbit, starting a new cycle.

The temperature distribution presented in Fig. 5b, for one-fourth of the plate, represents the steady-state conditions for the hot case, using the numerical models. The temperature distribution of the absorber plate, after it reaches the steady-state conditions during its low heat load conditions in the Earth's shadow, is almost flat (maximum variation of 0.20 K) and is not presented.

The average temperature of the plate and the net absorbed heat, for one-fourth of the plate, are plotted as a function of time in Fig. 9. Transition time is short. In practical terms two different steady-state conditions are achieved, for the sunny and for the shadowed portions of the orbit. The total absorbed heat by the plate is around 32 W for the sunny and zero for the shadowed parts of the orbit. This value is of the same order of magnitude obtained in the former USSR LHP experiments,[9] as mentioned in the literature review section.

Experimental Study

The main objective of the experimental work is to provide data to be compared with the analytical and numerical models and simulate,

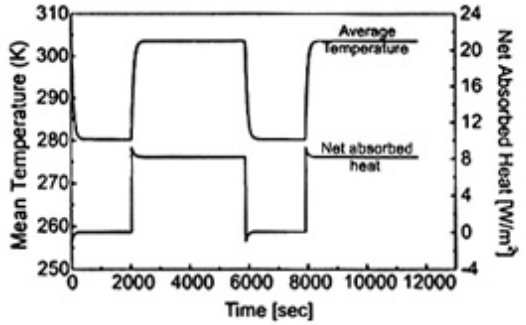

Fig. 9 Mean temperature and net absorbed heat as a function of time for one-fourth the absorber plate area.

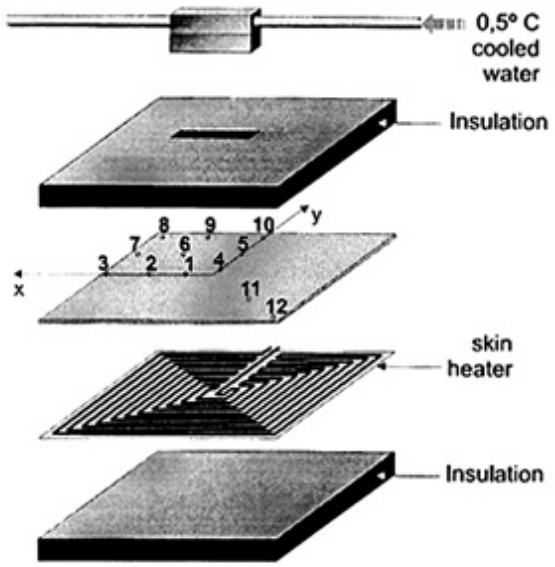

Fig. 10 Schematic of the experimental setup, indicating the position of the thermocouples.

as much as possible, the thermophysical conditions of an absorber plate subjected to the space radiation.

Figure 10 presents a schematic of the experimental setup. It consists basically of an aluminum plate of dimensions 0.02 × 0.02 × 0.00055 m, where a very thin skin heater is bonded over one of its faces. The skin heater is made of a nickel-chrome resistance, which is deposited over a Kapton sheet using printed circuit board technique. The total resistivity is 19.85 Ω. The heat generated by this resistance can be considered uniform, and it simulates the net heat absorbed (solar radiation minus emitted energy). This heat also accounts for the losses through the insulators and wires. Because of the material availability, the thickness of this plate is about half of that of the actual absorber plate to be used in the satellite.

The capillary pump was simulated by means of an aluminum parallelepiped of square section (19.15 mm of border and 61.15 mm of length) with a cylindrical hole inside. Another block, of similar dimensions (15.60 × 19.15 × 61.15 mm), was located between the capillary pump and the center of the plate. Cooling water, with temperature of around 0.5°C controlled by means of a thermal bath, flowed through the block. A thermal paste of high conductivity was spread over the contacting surfaces to minimize the thermal contact resistance. A neoprene rubber blanket, of 0.3 W/m K of thermal conductivity and dimensions 0.3 × 0.3 × 0.018 m, was used as the insulating material over both faces of the plate.

Twelve type K (Chromega-Alomega) thermocouples were installed (Fig. 10). A data acquisition system was used to acquire the temperature readings, and the resulting data were stored in a computer. The voltage and electrical resistances were measured by means of a high-precision digital voltmeter.

The following test procedure was adopted: cool water circulated within the capillary pump until the plate achieved steady-state conditions. Then, the power supply was turned on, and the electrical resistance released 32.65 W to the plate. After 45 min the power was turned off. After 45 min the cycle started again, being repeated four times. The data were acquired every 2 s.

According to Moffat,[18] the conceptual can be one of the major sources of errors in one experiment. In the present case the conceptual error arises because of the incapacity of the experimental setup to reproduce exactly the mixed boundary conditions prescribed in the physical model (see Fig. 3). In the setup an entire area between the block and the plate is at a known temperature, not just a border, as assumed for the theoretical models. Hence, the thermal constriction/spreading resistance is larger for the theoretical model than obtained experimentally. This effect decreases as the size of the plate increases. The difference between the experimental and theoretical temperatures depends on the plate region, being zero at the contact interface and reaching a maximum of +4°C on the corner. The numerical model was used in this estimation.

Another important source of error observed was the mounting error. In the present case this error affects especially the heat power generation readings. Heat can be lost to the environment because of the imperfect insulation of the rubber blanket. The average plate and insulation external temperatures were used in the calculation of the heat losses. These losses vary during the transient, but only two levels, for the hot and cold cases, are considered because the transient time is very short. The heat conducted through the insulation is −3.69 W (loss) for the hot case (sunny part of the orbit) and +2.26 W (gain) for the cold case (shadowed part of the orbit). The heat generated can also be lost by the electrical and the thermocouple wires. In this experiment several standard procedures, such as radiative thermal insulation and thermal grounding of the wires, were applied to reduce the heat transferred through the wires to the environment to around the negligible value of 1.94×10^{-3} W.

The measurement of temperature is not so simple as it could appear at first sight. Moffat[18] claims that the temperature reading errors can be divided in bias and random. The bias are the fixed errors that do not change during the tests, whereas the random are the unfixed errors that change as the measurements are taken.

The thermocouple installation procedure may cause one of the temperature bias errors. In the present case the Teflon-covered thermocouple wires were uncovered close to their beads. A small piece of Kapton tape is installed over the plate surface, where the temperature is acquired. The thermocouple bead is fixed in its final position over the Kapton by means of another Kapton tape. An aluminum tape, which area is similar to those of the Kapton tapes, is installed over the sandwich formed between the tapes and bead. The Kapton tape is an electrical insulator of the uncovered thermocouple wires and guarantees that the readings are taken exactly at the desired point. The aluminum tape insulates radiatively the thermocouple bead from the environment, and at the same time corrects for the optical properties modification effects of the thermocouple over the surface.

The data acquisition system introduces another bias error. For the present work the system was calibrated before the experiments, and, according to the manufacturer, the reading errors were $\pm 7.62 \cdot 10^{-2}$°C. Furthermore, the thermocouple manufacturer reports that the Type K thermocouple measures temperatures with a bias error of ±1.1°C. The milivoltages generated by the thermocouple are converted in temperatures by means of an equation supplied by the manufacturer, with an error of ±0.7°C. All of these bias errors are rms combined, resulting in $B = \pm 1.31$°C. One way of minimizing the bias errors would be the calibration of each of the thermocouples used. This effort would not work for the present case because the reading errors are smaller than the conceptual errors. The main source of random errors observed is the electrical noise in the data acquisition system. This error is minimized, as much as possible, using the well-known electrical grounding procedures.

The steady-state regime was considered achieved when the largest measured temperature variation was less than 1°C in 1 min. A large number of measurements (around 550) were taken after the system reached this condition. The standard deviation S was obtained from this large sample. Based on the bias and random errors, a 95% confidence level uncertainty interval was established [$U^2 = B^2 + (t_{0.95}S)^2$, where $t_{0.95}$ is the student distribution coefficient[19,20]]. A value of 4°C was added to the maximum uncertainty limit to account for the already-mentioned conceptual error. The uncertainty associated with all data is shown in vertical bars in the graphs presented in Fig. 11.

The temperatures vary with time in the transient regime, so that only one temperature can be obtained at a time. As the cycle was repeated four times, the transient sample has four elements ($N = 4$, $df = 3$, and $t_{0.95} = 3.182$). The 95% confidence level uncertainty interval was obtained for the samples (one sample each 2 s) of four elements (temperature measurements), which were acquired during the test. Some of these intervals are presented in the graphs shown in Fig. 11.

The heat power dissipated in the plate is determined from the voltage and the electrical resistance data. According to the multimeter manufacturer, the electrical resistance bias error is ±0.002 Ω, and the voltage bias error is ±0.003 V. These two errors were propagated into the power expression ($P = V^2/R$), resulting in a bias error of ±0.00837 W. The voltage and the resistance measurements were stable along the test, so that the standard deviation of the electrical power is zero. Four measurements of power dissipation were obtained (one for each cycle), and, therefore, the 95% uncertainty interval is 32.648 ± 0.00837 W with $t_{0.95} = 3.182$, as before.

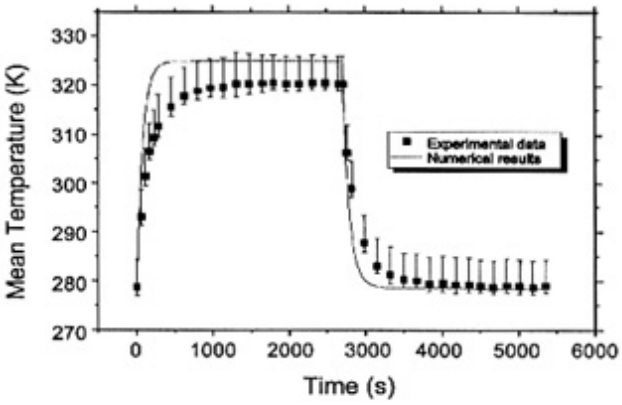

Fig. 11 Comparison between the mean numerical and experimental temperatures.

Comparison Between Experimental and Theoretical Results

For better comparison between experimental and theoretical data, the net heat power, as given in the last section, is used. This power is simply substituted in the analytical model equations. For the numerical case the net absorbed heat is the output of the model, whereas the incident solar energy S is the input. Therefore, this value has to be adjusted until the absorbed heat calculated is equivalent to the experimental values. For the analytical model the values 28.76 and 2.26 W were used for the hot and cold parts of the test. For the numerical model the values of 28.52 and 2.20 W were obtained after several iterations.

Figure 12 presents the comparison between the experimental, analytical, and numerical temperature results for the cold (empty symbols) and hot (full symbols) cases, for the thermocouples shown in Fig. 10. The thermocouple number 4 presented problems, and its readings are not shown. The comparison between the theoretical (analytical and numerical) and experimental results is very good, within −0.7 and 4.0% for the hot case and within −0.5 and 0.3% for the cold case. The comparison of the experimental data with the numerical results is better than the comparison with the analytical data, as expected. For the hot steady-state case the differences between the numerical and experimental temperatures read by the thermocouples located near the capillary pump (numbers 2 and 5) are so small that the predicted temperatures are within the uncertainties limits. The comparison for the thermocouples close to the plate corners (numbers 7–9) is not so good. On the other hand, the difference between the analytical and numerical results are almost constant for all of the thermocouple positions. Figure 12 also shows that all of the results agree very well among themselves for the cold case.

In Fig. 11 the area weighted mean numerical temperatures (full line) for a complete orbit, including the transient and steady-state regimes, are compared with experimental data. This figure shows that the steady-state numerical results are located within the uncertainty limits of the experimental data, indicating that the comparison is very good. The comparison plots of the numerical and experimental temperatures for all of the thermocouples are very similar to the graph of Fig. 11 and will not be presented in this paper. The temperature experimental uncertainties (vertical bars) represent only around 1.6 and 1.4% of the temperatures for the cold and hot cases, respectively.

Figure 11 also shows that the experimental steady-state conditions are reached much slower than the theoretical predictions. Actually, the theoretical model considers radiation heat exchange, whereas in the experiment the heat is released to the plate by conduction. Radiation heat exchanges are very sensitive to the temperature level.

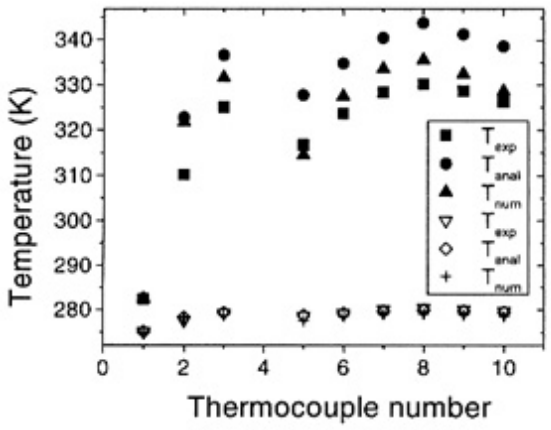

Fig. 12 Comparison between theoretical (analytical and numerical) results and experimental data for the thermocouples located according to Fig. 10.

When the satellite just enters in the Earth shadow, the plate is still hot and able to release heat to space quickly. Similarly, when the satellite leaves the shadow, the plate is cold allowing the sun energy to be absorbed quickly. However, in the experimental setup the variation of the thermal conductivity of the material with the temperature is negligible, and the simulated heat absorption capacity is not affected by the temperature levels.

The transient numerical model was selected as the theoretical model for comparison with data for the only reason that it represents better the physical model tested and that it is able to estimate the transient behavior.

Conclusion

Small scientific satellites generally do not provide enough power to run many experiments in space. An efficient way to deal with this problem is to use the solar energy. Outside panels of the satellite can be used as absorber plates. This work shows that solar energy can be absorbed by an absorber plate, made of a black-painted thin aluminum sheet.

The amount of absorbed heat depends on the plate temperature level. Therefore, the temperature distribution must be known to enable the evaluation of this energy. In this paper this temperature distribution is determined by three different ways. Based on a common physical model, one analytical (steady-state) and two numerical (steady-state and transient) models are developed. An experimental setup is designed and tested with the objective of collecting data to be compared with the theoretical models. This comparison is very good, especially between the experimental and numerical results.

The analytical model was shown be simpler to work with because any result can be obtained by the direct substitution of the appropriate physical parameters. In spite of being more time and computer consuming, the numerical model was shown to be more precise because some restrictive hypotheses imposed to the analytical model were not applied to the numerical model. In fact, both the models proved to be very efficient in the estimation of the plate temperature distribution and of the net absorbed heat. In conclusion, the use of solar absorbers for experiments in space was shown to be an easy, light, and efficient solution for heat generation problems in small satellites.

References

[1]Chalmers, D. R., Pustay, J. J., Moy, C. B., and Kroliczek, E. J., "Application of Capillary Pumped Loop Heat Transport Systems to Large Spacecraft," AIAA Paper 86-1295, June 1986.

[2]Ku, J., Kroliczek, E. J., and Butler, D., "Capillary Pumped Loop GAS and Hitchhiker Flight Experiments," AIAA Paper 86-1249, June 1986.

[3]Delil, A. A. M., Heemskerk, J. F., Dubois, M., van Oost, S., Supper, W., and Aceti, R., "In-Orbit Demonstration of Two-Phase Heat Transport Technology: TPX/G-557 Flight Results," Society of Automotive Engineers, Paper 941404, June 1994.

[4]Butler, D., and Hoang, T., "The Enhanced Capillary Pumped Loop Flight Experiment: A Prototype of the EOS Platform Thermal Control System," AIAA Paper 91-1377, June 1991.

[5]Butler, D., Ottenstein, L., and Ku, J., "Design Evolution of the Capillary Pumped Loop Flight Experiment," Society of Automotive Engineers, Paper 961431, July 1996.

[6]Ottenstein, L., and Nienberg, J., "Flight Testing of the Two-Phase Flow Flight Experiment," Society of Automotive Engineers, TP 981816, July 1998.

[7]Baker, C. L., Bienert, W. B., and Ducao, A. S., "Loop Heat Pipe Flight Experiment," Society of Automotive Engineers, TP 981580, July 1998.

[8]Ku, J., Ottenstein, L., Cheung, K., Hoang, T., and Yun, S., "Ground Tests of Capillary Pumped Loop (CAPL 3) Flight Experiment," Society of Automotive Engineers, TP 981812, July 1998.

[9]Maidanik, Y. F., Fershtater, Y. G., and Goncharov, K. A., "Capillary-Pump Loop for the Systems of Thermal Regulation of Spacecraft," *Proceedings of the 4th European Symposium on Space Environmental and Control Systems*, 1991, pp. 87–92.

[10]Goncharov, K. A., Nikitkin, M. N., and Golovin, O. A., "Loop Heat Pipes in Thermal Control Systems for 'OBZOR' Spacecraft," Society of Automotive Engineers, TP 951555, July 1995.

[11]Bazzo, E., and Mantelli, M. B. H., "Study of Design Parameters of a Small Scale CPL," Society of Automotive Engineers, TN 981690, July 1998, pp. 1–8.

[12]Bazzo, E., Mantelli, M. B. H., Vlassov, V., and Ochterbeck, J. M., "Proposed Conception of a Small Scale CPL for Testing Under Microgravity," *Proceedings of the 4th International Symposium of Small Satellites and Systems*, 1998, pp. 1–13.

[13]Gilmore, D. G., *Satellite Thermal Control Handbook*, 1st ed., Aerospace Corp. Press, El Segundo, CA, 1994, pp. 2.3–2.31.

[14]Couto, P., and Mantelli, M. B. H., "Environmental Heat Loads Over External Plates of a Microgravity Capillary Pumped Loop Experiment," *Proceedings of VI PACAM (Pan American Conference of Applied Mechanics)*, 1999, pp. 1–4.

[15]Mantelli, M. B. H., and Bazzo, E., "Modeling of Temperature Distribution of Solar Absorbers for Space Applications," *Proceedings of the 10th International Heat Pipe Conference*, 1997.

[16]Arpaci, V. S., *Conduction Heat Transfer*, 1st ed., Addison Wesley Longman, Reading, MA, 1966, pp. 219, 220.

[17]Ozisik, M. N., *Heat Conduction*, 2nd ed., Wiley, New York, 1993, pp. 6–16.

[18]Moffat, R. J., "Describing the Uncertainties in Experimental Results," *Experimental Thermal and Fluid Science*, Vol. 1, Elsevier, New York, 1988, pp. 3–17.

[19]Kline, S. J., and McClintock, F. A., "Describing the Uncertainties in Single-Sample Experiments," *Mechanical Engineering*, Jan. 1953, pp. 3–8.

[20]Granger, R. A., *Experiments in Fluid Mechanics*, 1st ed., Holt, Rinehart, and Winston, Philadelphia, 1988, pp. 467–481.

I. D. Boyd
Associate Editor